Microscopic Mechanisms of the Brittleness of Viscoelastic Fluids

H. Tabuteau, S. Mora,* G. Porte, M. Abkarian, and C. Ligoure

Laboratoire des Colloïdes, Verres et Nanomatériaux, UMR 5587, Université Montpellier 2 and CNRS, Place Eugène Bataillon, F-34095 Montpellier Cedex, France

(Received 27 October 2008; published 14 April 2009)

We show that a large class of viscoelastic fluids, i.e., transient networks, are brittle according to the Griffith's theory of solid fracture. However, contrary to solids, cracks are intrinsic to the material arising from the equilibrium nature of the fluid microstructure. The brittleness of these fluids comes from thermal fluctuations of bonds distribution. In this approach, the rupture stress is predicted to be on the order of the Young modulus, in very good agreement with experimental values.

DOI: 10.1103/PhysRevLett.102.155501 PACS numbers: 62.20.mj, 83.10.Bb, 83.50.Jf

In principle liquid liable to fracture in a brittle manner should possess a structure capable of transmitting elastic forces over macroscopic scales. But this structure should also be labile and reversible to let the material flow. The fracture of fluids should only be observed for high rates of deformation for which the fluid cannot relax, the material responding in a solidlike manner. Such behavior was recently reported by Gladden with micellar fluids [1]. This phenomenon is also well known as cohesive failure in the polymer literature [2], and its consequences on flow properties have been extensively reported [3,4]. However, the microscopic mechanisms of fracture nucleation are still unknown. Here we investigate fracture nucleation in a model viscoelastic fluid. We provide strong evidence of the brittleness of this material in the framework of Griffith's theory of brittle fracture. We show that such fluid can fail in a brittle manner because microcracks, present within the material, lower the overall strength, as in real solids. Moreover, by identifying thermal fluctuations of the bonds distribution within the materials with microcracks, we explain the unexpected low value of the surface tension associated with the fracture; this leads to the prediction that the critical rupture stress is on the order of the Young modulus, in agreement with the experimental results.

We used a model system made of oil-in-water droplet microemulsion connected to each other by telechelic polymers [5]. The droplets are swollen with decane, stabilized by a cationic surfactant (cetyl-pyridinium chloride) and a cosurfactant (*n* octanol), and also dispersed in brine (0.2*M* NaCl). The telechelic polymer have a hydrophilic backbone [poly(ethylene) oxide], with a hydrophobic group (eighteen CH_2 groups) at both ends. These end chains stick reversibly into the hydrophobic core of the oil droplets and can either decorate (loop) or link (bridge) the droplets, leading to a self-assembled structure, Fig. 1. We define the connectivity r as the average number of hydrophobic stickers per droplet. Far above from the percolation threshold [6] this model system behaves as an elastic network with a shear modulus [7] $G_0 = nk_BT$ (n is the number density of linking chains, k_B the Boltzman's constant, T the temperature). The adhesion energy of a sticker in oil droplets is moderate ($\sim 20k_BT$) so that it randomly escapes from time to time and reconnects to any accessible droplet and the topology of the network is permanently renewed, allowing stress relaxation and flow. These telechelic based systems provide ideal experimental realizations of the notion of transient networks [7,8] with a Maxwell model as a constitutive equation characterized by G_0 and a single relaxation time τ [9], related to the life time of the cross-links. We have measured those two quantities (G_0 and τ) by standard linear rheological tests performed with an Ares-RFS controlled-strain rheometer at 23 °C. Consistently with the Maxwell model, the shear stress σ_{yz} measured in a steady state increases linearly with the shear rate $\dot{\gamma}$ ($\sigma_{yz} = G_0\tau\dot{\gamma}$) and the first normal stresses difference ($N_1 \equiv \sigma \equiv \sigma_{zz} - \sigma_{yy} = 2G_0\tau\dot{\gamma}^2$) quadratically, Fig. 2. However, above a critical stress, the flow curve exhibits a sharp discontinuity and at the same time, fractures open up all around the sample and grow rapidly. It is worth noting that the fractures are tilted 45° from the shear plane, perpendicular to the direction of the maximum extension, Fig. 2. Furthermore, this happens inside the linear flow regime ($\dot{\gamma}\tau < 1$). Interestingly, these fractures appear at a critical rate such that N_1 is larger than σ_{yz}

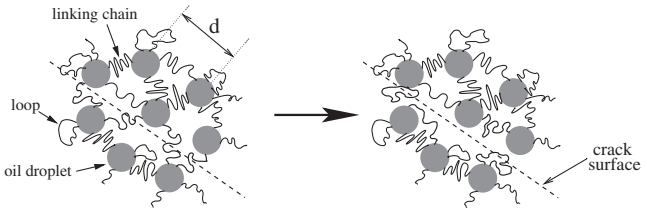

FIG. 1. Schematic of a bridged microemulsion. The telechelic polymers can either link two oil droplets or loop on a single one. (Left) Before the crack nucleation (bold dashed line) polymers can bridge oil droplets on both side of the bold dashed line. (Right) When the crack occurs, the same polymers cannot cross the bold dashed line anymore and form bridges in the other directions.

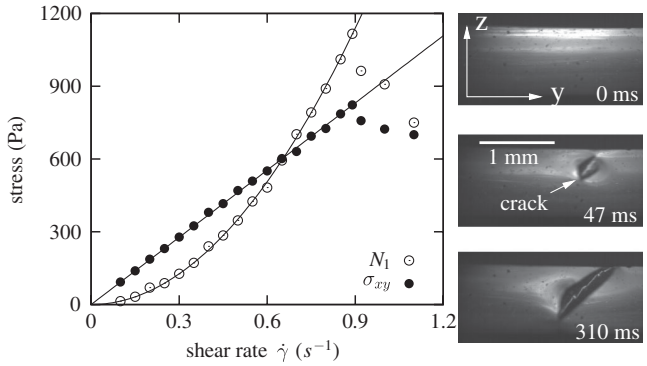

FIG. 2. (Left) shear stress (σ_{yz}) and normal stress ($N_1 = \sigma_{zz} - \sigma_{yy}$) versus shear rate for a bridged microemulsion with $r = 9$. The continuous lines are fits (Maxwell model). (Right) Development of a fracture, occurring at the surface of the sample, for a shear rate equal to 0.8 s^{-1}, corresponding to the critical normal stress $\sigma = 1190$ Pa.

indicating that the tensile stress rather than the shear stress triggers the phenomenon, a systematic feature of brittle fracture in solids. But in contrast to solids, here the fractures heal over rapidly after the shear rate is switched off, and a new experiment can be performed after a few minutes with quantitatively the same behavior. A brittlelike fracture is also observed with the same fluid in a purely extensional flow during a pendant drop experiment monitored with a fast camera (FastCam Photron), equipped with a macrolens, Fig. 3(a). A syringe pump (KDS 200 Scientific) was used to form the drops with a fixed volume of 50 μl and a constant rate of 2 ml/h for all the solutions. The fluid initially in the syringe flows through a lower plastic tube of diameter of 2.60 mm and a drop emerges at the tube outlet which is enclosed in a glass box to reduce air currents. During the experiment, the tensile stress steadily increases as the cylindrical body of the drop thins up. At any time, the recorded extension rate $\dot{\epsilon}$ as a function of the effective extensional stress σ agrees with the Maxwell model: the extensional viscosity at moderate rate is found three times larger than the shear viscosity ($\sigma \simeq 3G_0\tau\dot{\epsilon}$). But suddenly again, inside the linear regime ($\dot{\epsilon}\tau \simeq 0.2$), a fracture nucleates and propagates across the sample which leads to the rupture of the drop; see Fig. 3(b) and movie 1 in the supplementary material [10]. We got the critical stress at the rupture of the drop σ in the following way. We measured the diameter of the drop where the fracture occurs and we weighted the mass of the falling part with accuracy 1 mg. So the stress σ_{zz} is measured with a precision of 5%. Finally, the stress at the rupture is equal to $\sigma_{zz} - \sigma_{yy}$ with σ_{yy} the radial stress corresponding to the Laplace pressure. It is worth noting that upon growing, the fracture exhibits the parabolic shape [Fig. 3(c)] expected for an elastic solid breaking under tension [11,12]. Indeed, on the time scale of the rupture, which is much shorter than the relaxation time (1 s), the material is responding in a solidlike manner. Finally, fractures are observed when inflating an air bubble in the bulk of the viscoelastic fluid; see Fig. 4 and movie 2 in the supplementary material [10]. During this experiment a bubble grows at a fixed pressure (imposed by a MFCS-4C device, Fluigent, Paris, France)

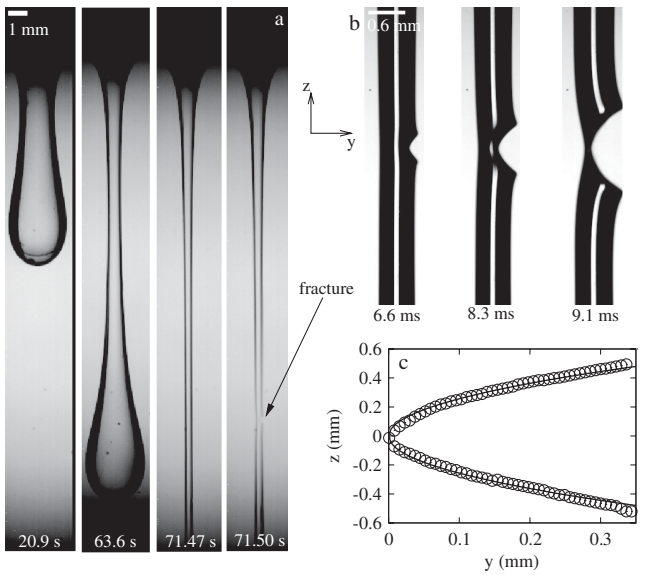

FIG. 3. (a) Elongation of a drop of a solution of bridged microemulsion ($r = 9$) under gravity. The fracture occurs at the surface of the filament. The critical measured tensile stress is $\sigma = 1720$ Pa. (b) Zoomed images of the same fracture which propagates across the sample. (c) Typical fracture profile corresponding to the picture b (middle one) (circles). The black line represents a power law $u(x) \propto \sqrt{x}$.

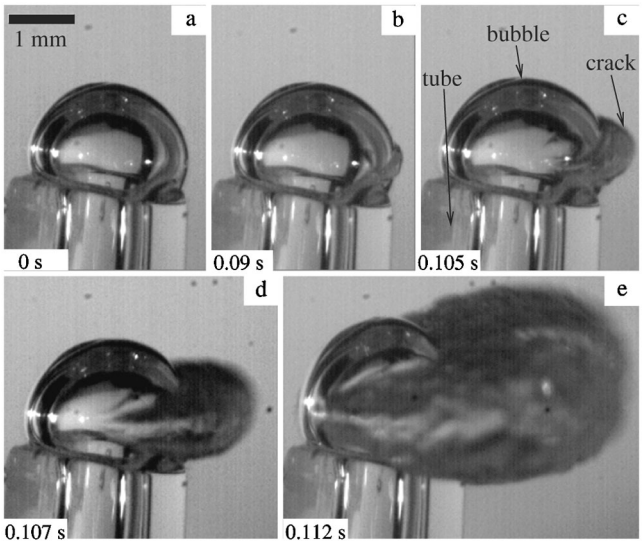

FIG. 4. (a) Bubble growth at a fixed pressure 2000 Pa inside the same solution as in Fig. 2. (b) A disklike fracture appears at the bubble surface. (c),(d),(e) Fracture propagation. The critical pressure is equal to 1800 Pa which gives a critical stress (after taking into account the Laplace pressure ~160 Pa) equals to 1640 Pa.

from the outlet of a capillary tube (diameter 0.8 mm) into the fluid. At moderate excess pressure of air injection ΔP (above atmospheric pressure), the bubble grows progressively. But when ΔP exceeds a critical value, a flat disklike crack suddenly arises at an arbitrary point onto the bubble surface and grows explosively, sharply cutting apart the sample. If ΔP is released back below its critical value, the fracture heals spontaneously. Interestingly, for sufficiently large bubble the critical tensile stress (σ) at the bubble surface is identical to the excess air pressure $\sigma = \Delta P$, whose value is comparable to those obtained in the two other geometries.

In each experiment presented here, the fracture mechanism is a two step process. In the following, it will be shown that the first step consists in the spontaneous nucleation of a wet fracture starting up from a lack of cohesion of the network, the microcrack being filled up with solvent. The second step corresponds to the destabilization of the capillary bridge, driving eventually to the dry fracture with parabolic profile as displayed in Fig. 3(b). This last step and the properties of the fracture propagation will be described in detail elsewhere. In the following, we focus only on the first step, i.e., the fracture nucleation.

These three experimental facts present strong analogies with the fracture of brittle solids: the rupture suddenly appears within the linear regime, it is driven by the tensile stress, and it exhibits a parabolic profile in the extensional test. It is therefore tempting to extend the Griffith's theory of brittle fracture [13] to the present transient network. The Griffith's point of view starts up with preexisting microcracks and considers the energy required for them to grow spontaneously under a given constant stress. A surface energy has to be paid to break more cohesive bonds, counterbalanced by the bulk elastic energy released by the opening of the crack. For a given stress σ the Griffith energy cost W for a crack of size L reads then

$$W(\sigma, L) = \frac{\pi}{2} L^2 F_s - \alpha \frac{\pi L^3 \sigma^2}{6Y}, \tag{1}$$

with L the size of a disklike crack, F_s the cohesive energy per unit area, $Y = 3G_0$ the Young modulus, and $\alpha \simeq 1$ a constant depending on geometrical factors. The stress σ being fixed, $W(\sigma, L)$ reaches a maximum:

$$W_{\max}(\sigma) = \frac{2\pi}{3\alpha^2} \frac{F_s^3 Y^2}{\sigma^4} \tag{2}$$

for a crack size (the so-called Griffith length) $L_c(\sigma) = \frac{2}{\alpha} \times \frac{F_s Y}{\sigma^2}$. For a crack size larger than L_c, $dW/d\sigma < 0$, leading to a catastrophic growth of the crack, in contrast with a crack size smaller than L_c. In brittle solids, microcracks are formed irreversibly during the material processing. Upon increasing the applied stress the largest among them becomes critical and leads to fracture. In our case, however, the elastic network results from an equilibrium self-assembly of bonds, with a thermally activated size distribution of domains without polymers connecting droplets that we *identify* with microcracks. Pomeau [14] suggested that the Griffith's energy [Eq. (1)] can be viewed as an energy barrier of height $W_{\max}(\sigma)$ that can be overcome by thermal fluctuations according to Kramers theory. This occurs as soon as $W_{\max}(\sigma_c) \leq k_B T$. Then, from Eq. (2), a fracture appears for $\sigma \geq \sigma_c$ with

$$\sigma_c = \left(\frac{2\pi}{3\alpha^2} \frac{F_s^3 Y^2}{k_B T} \right)^{1/4}. \tag{3}$$

This approach has been used to interpret fracture nucleation in 2D microcrystals [15], gels [16], and heterogeneous materials [17]. However, it was not able to explain all the experimental features [17]. In these experiments, microcracks are not reversible. This is in strong contrast with our system, where the use of Pomeau's theory is here fully justified because microcrack size distribution is entirely controlled by thermal energy fluctuations (healing and growth are both possible). In order to calculate σ_c from Eq. (3), we need a precise estimate of the surface energy F_s. The microcracks appear well before the fracture forms an interface with air, Fig. 3. A microcrack corresponds to a surface across which there is no connection between oil droplets. The crack is completely wet by the aqueous solvent and the only contribution to F_s comes from the polymer network.

At first sight, such a crack requires some stickers to be pulled out of the oil droplets and dangle free into the solvent. But in fact a crack can be achieved at a much lower energy cost corresponding to the lack of accessible configurations of the polymers which face the crack surface. These cracks always exist, in the fluid, due to equilibrium thermal fluctuations. In the vicinity of a crack, polymers do not cross the crack surface and therefore lose roughly half of the configurations they would have had if they were far from the crack surface, Fig. 1. So the free energy cost associated to the crack is $k_B T \ln 2$ per active polymer. Therefore the surface energy can be written as $F_s = \frac{fr}{2d^2} k_B T \ln 2$, where r is the average number of hydrophobic stickers per droplet (connectivity), f is the average fraction of bridging configurations for a given polymer ($f \sim 0.5$ [18]), and d is the center-to-center distance between droplets $d = [(4\pi/3)/\phi]^{1/3} r_0$ (ϕ and r_0 are the volume fraction and the oil droplet radius, respectively). The typical value of F_s is extremely low and roughly equal to 10 μJ m^{-2}. Knowing the surface energy F_s, we are able to calculate the critical stress σ_c [Eq. (3)], above which the fracture occurs:

$$\sigma_c = \left[\frac{3}{\pi\alpha^2} \left(\frac{f \ln 2}{4} \right)^3 \phi^2 \frac{r^3}{r_0^6} \right]^{1/4} (k_B T Y)^{1/2}. \tag{4}$$

Since far from the percolation threshold the Young modulus is roughly equal to $Y = 3nk_B T$ where $n = 3\phi r f/(4\pi r_0^3)$, we eliminate ϕ and r_0 in Eq. (4) which

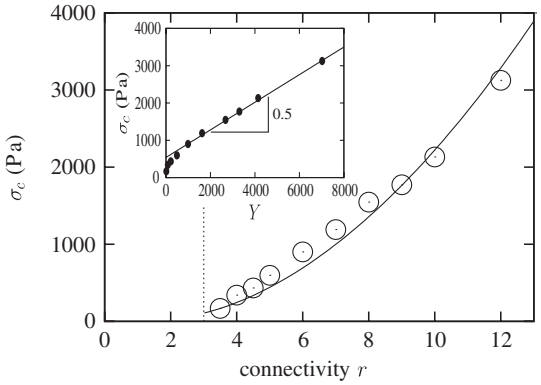

FIG. 5. Plot of the rupture stress coming from the pendant drop experiments (circles) and the expected values from Eq. (4) as a function of the connectivity r. f has been fixed to its expected value: $f = 0.5$. The only free parameter is $\alpha = 0.9$ ($\alpha \sim 1$ as expected). The vertical dashed line corresponds to the percolation threshold ($r = 3$). The inset gives the variation of the experimental rupture stress with the Young modulus, corresponding to the different connectivity. Note that the observed deviation of σ_c from its linear dependence with Y observed at small r, originates from the vicinity of the percolation threshold [5].

can then can be approximated by $\sigma_c \simeq ([(\frac{\ln 2}{3})^3 \frac{\pi}{4\alpha^2} rf]^{1/4} Y$. For typical values of f and r, the prefactor in remains of the order of unity: $\sigma_c \sim Y$ (far from the percolation threshold). Figure 5 shows that the critical stresses measured during the pendant drop experiment are in very good agreement with the ones derived from our simple approach [Eq. (4)], when the polymer concentration changes (r increases), at a fixed volume fraction of droplets. This result confirms the physical basis of the surface energy we have chosen. In this respect, we checked that the measured critical stress is mostly independent of the length of the sticker (twenty-one versus 18 CH_2 groups) and therefore of the adhesion energy. We also obtained two other results consistent with the classical picture of brittle fracture. (i) The Griffith's length is for all the samples of the order of 3 times the distance between two oil droplets. (ii) The rupture occurs in the linear regime: $\sigma_c \simeq 0.5Y$, Fig. 5.

We have shown that the main ingredients of brittleness of the fluid are bonds reversibility and fracture surface energy resulting from the configurational entropy of the bonds. These features being shared by most complex fluids (associating polymers solutions [19], fibrillar networks [20], supramolecular rubber [21], and actin gels reminiscent of cell cytoskeleton [22]), or even entangled solution of wormlike micelles the brittleness of soft material might be general.

We thank T. Phou and R. Aznard for polymer synthesis, M. Ciccotti, W. Kob, and L. Berthier for stimulating discussions. Work conducted in the framework of the Network of Excellence *SoftComp* supported by the EU. This work has also been supported by ANR under Contract No. ANR-06-BLAN-0097 (TSANET).

*smora@univ-montp2.fr

[1] J. Gladden and A. Belmonte, Phys. Rev. Lett. **98**, 224501 (2007).
[2] A. Malkin and C. Petrie, J. Rheol. (N.Y.) **41**, 1 (1997).
[3] J. Hutton, Nature (London) **200**, 646 (1963).
[4] H. Mizunuma and H. Takagi, J. Rheol. (N.Y.) **47**, 737 (2003).
[5] M. Filali, R. Aznar, M. Svensson, G. Porte, and J. Appell, J. Phys. Chem. **103**, 7293 (1999).
[6] E. Michel, F. Molino, J. Kieffer, and G. Porte, J. Rheol. (N.Y.) **45**, 1465 (2001).
[7] F. Tanaka and S. Edwards, J. Non-Newtonian Fluid Mech. **43**, 273 (1992).
[8] M. Green and A. Tobolsky, J. Chem. Phys. **14**, 80 (1946).
[9] C. Macosko, *Rheology: Principles, Measurements and Applications* (Wiley-VCH, New York, 1994).
[10] See EPAPS Document No. E-PRLTAO-102-075917 for fracture propagation movies. For more information on EPAPS, see http://www.aip.org/pubservs/epaps.html.
[11] J. Greenwood and K. Johnson, Philos. Mag. A **43**, 697 (1981).
[12] G. Barenblatt, Adv. Appl. Mech. **7**, 55 (1962).
[13] A. Griffith, Phil. Trans. R. Soc. A **221**, 163 (1921).
[14] Y. Pomeau, C.R. Acad. Sci. Ser. II **314**, 553 (1992).
[15] L. Pauchard and J. Meunier, Phys. Rev. Lett. **70**, 3565 (1993).
[16] D. Bonn, H. Kellay, M. Prochnow, K. Ben-Djemiaa, and J. Meunier, Science **280**, 265 (1998).
[17] A. Guarino, S. Ciliberto, A. Garcimartín, M. Zei, and R. Scorretti, Eur. Phys. J. B **26**, 141 (2002).
[18] V. Testard, J. Oberdisse, and C. Ligoure, Macromolecules **41**, 7219 (2008).
[19] A. Tripathi, G. H. McKinley, K. Tam, and R. Jenkins, Macromolecules **39**, 1981 (2006).
[20] P. Terech and R. Weiss, *Molecular Gels: Materials with Self-Assembled Fibrillar Network* (Springer, Secaucus, 2006).
[21] P. Cordier *et al.*, Nature (London) **451**, 977 (2008).
[22] A. A. R. Bausch and K. Kroy, Nature Phys. **2**, 231 (2006).